Comparison of Laser Coordinate Measurements and Hierarchical Multiscale Finite Element Models for the Cup Drawing of Three Commercial Aluminum Alloys

Pichardo, Diego Ricardo; Ramírez, Miguel Ángel; Kestens, Leo A.I.; Van Bael, Albert; Schouwenaars, Rafael

DOI
10.1007/978-3-031-58006-2_26

Publication date
2024

Document Version
Final published version

Published in
Numerical Methods in Industrial Forming Processes

Citation (APA)
Pichardo, D. R., Ramírez, M. Á., Kestens, L. A. I., Van Bael, A., & Schouwenaars, R. (2024). Comparison of Laser Coordinate Measurements and Hierarchical Multiscale Finite Element Models for the Cup Drawing of Three Commercial Aluminum Alloys. In J. Kusiak, Ł. Rauch, & K. Regulski (Eds.), *Numerical Methods in Industrial Forming Processes: Numiform 2023* (pp. 337-346). (Lecture Notes in Mechanical Engineering). Springer. https://doi.org/10.1007/978-3-031-58006-2_26

Comparison of Laser Coordinate Measurements and Hierarchical Multiscale Finite Element Models for the Cup Drawing of Three Commercial Aluminum Alloys

Diego Ricardo Pichardo, Miguel Ángel Ramírez, Leo A. I. Kestens, Albert Van Bael, and Rafael Schouwenaars

Abstract Cup drawing is a benchmark experiment frequently used to validate anisotropic constitutive models and multiscale crystal plasticity codes for yield locus prediction. Earing of the cup rim and thickness variation along the cup wall are sensitive to plastic anisotropy. This test was implemented on an industrial forming press and applied to 85 mm diameter disks of commercial AA1100, AA3103, and AA5005 alloy sheet. Cup geometry was determined using a laser probe coordinate measurement machine (CMM). Finite element models (FEM) were developed with ABAQUS Explicit software and a user-defined subroutine for the anisotropic yield locus based on the hierarchical multiscale model (HMS). As the coordinate cloud produced by the CMM is unrelated to the nodes of the deformed FEM-mesh, both were fitted to a polynomial-Fourier series expansion. After cleaning and correction of the CMM

D. R. Pichardo · M. Á. Ramírez · R. Schouwenaars (✉)
Departamento de Materiales y Manufactura, Facultad de Ingeniería, Edificio O, Universidad Nacional Autónoma de México. Avenida Universidad 3000, Coyoacán 04510, Ciudad de México, México
e-mail: raf_schouwenaars@yahoo.com

M. Á. Ramírez
Centro Tecnológico Aragón, Facultad de Estudios Superiores Aragón, Universidad Nacional Autónoma de México, Av. Rancho Seco S/N, Col. Impulsora, Cd. Nezahualcóyotl 57130, Estado de México, México

L. A. I. Kestens · R. Schouwenaars
Department of Electromechanical, Systems and Metals Engineering, Ghent University, Technologiepark 46, 9052 Ghent, Belgium

L. A. I. Kestens
Department of Materials Science and Engineering, Delft University of Technology, Mekelweg 2, 2628 Delft, CD, Netherlands

A. Van Bael
Department of Materials Engineering, KU Leuven, Kasteelpark Arenberg 44/Box 2450, 3001 Leuven, Belgium

J. Kusiak et al. (eds.), *Numerical Methods in Industrial Forming Processes*, Lecture Notes in Mechanical Engineering, https://doi.org/10.1007/978-3-031-58006-2_26

data, point-by-point comparison can be performed between model and experiment. For AA1100, the position of the ears was correctly identified but their magnitude was underestimated. Excellent coincidence was found for AA5005, with strong ears at 0 and 90°. The small ears at -30° and 30° and secondary ears at 90° were correctly predicted for AA3013.

Keywords Cup drawing · Aluminum alloy · Coordinate measurement · Yield locus · Multiscale modeling

1 Introduction

Modeling of metal forming processes has become an indispensable instrument in industry. It allows for drastic reductions in the lead-up times for process development and in the costs associated with tool building and retooling [1]. While bulk forming processes can often be modeled with the isotropic von Mises yield criterion, this is not the case for sheet forming, where anisotropy plays an important role [2, 3].

An extensive overview of the different yield loci, physical and virtual test methods and the crystal plasticity models used in virtual experiments was given in the framework of ESAFORM [4], where 11 teams tested the accuracy of finite element models for the cup-drawing of a 6016-T4 aluminum sheet. Elements for the validation were the prediction of yield stress and *r*-values in different directions in the sheet, cup height, earing amplitude, and the force–displacement curve during the process.

Cup drawing has been popular to test the accuracy of proposed yield loci because it provides a simple example of industrial deep-drawing processes. Early models [5, 6] introduced anisotropy in existing continuum models for cup drawing [7] and validated by manually measured cup heights at determined positions of the cup rim [8]. Full constraints and relaxed constraints' Taylor models [9] were tested; Engler followed a similar approach based on the VPSC model [10, 11]. Neither of these studies involved the formal definition of an anisotropic yield locus nor the use of FEM. Generally, the global shape of the cup profile was predicted in a satisfactory manner, but the absolute cup height was not studied in detail.

Early efforts to incorporate an anisotropic yield locus into FEM based on a polynomial fit to virtual experiments were provided by Van Houtte et al. [12] and Munhoven et al. [13]. These papers focused more on the technical aspects and proof of concept than on the precision of the results. Consecutive versions of Barlat's yield criteria [3, 4, 14] have been incorporated into FEM and applied to cup drawing by Yoon et al. [15–17] and Han et al. [18], who incorporated virtual experiments based on the CPFEM [19] to analyze the effect of texture evolution.

A hierarchical multiscale (HMS) [20] approach was used by Ramírez et al. [21] to model cup drawing on two AA6016 alloys with different sheet thicknesses. HMS uses the ALAMEL crystal plasticity model [9] to execute the virtual experiments required to fit the FACET [22] yield locus. Good coincidence was found in terms of earing profile, but average cup height depended critically on the friction coefficient.

The latter value also affects the punch force, although to a lesser extent. A significant effect was found by modeling the tools as elastic solids, contrary to the generally used approximation of perfectly rigid tools. This work expands the latter study by analyzing three commercial Al-alloy sheets with significantly different textures.

2 Experimental Set-Up

The alloys used are commercial AA1100-O, AA3103-O, and AA5005-O. Tensile curves were measured according to ISO 6892–1:2016. Only the results in the rolling direction (RD) are required in HMS. Tensile curves were fitted to a Voce hardening law. X-ray texture measurements were performed on a Siemens D500 texture goniometer. The orientation distribution function (ODF) was determined using four incomplete (111), (200), (220), and (311) pole figures measured with the reflection method [23]. The ODFs were calculated using the series expansion method [24] with $L_{max} = 22$, considering the orthorhombic sample symmetry of the sheet. Representative ODF sections are shown in Figs. 1, 2 and 3, using the Bunge convention for Euler angles.

Cup drawing experiments were performed on a 75 T mechanical press (Meister, Germany). The press and tool assembly are shown in Fig. 4. The punch velocity, as measured from the load cell signal, is 50 mm/s. The tool geometry follows ISO 11531:2015. One important difference with a hydraulic system is that the blank holder force is imposed by springs and is not constant during the operation. The geometry of the cups was measured with a FARO laser line probe mounted on a FARO-arm (FARO Inc., Rochester, NY).

The finite element model was described in Ref. [21], but wall thickness was rescaled from 1.1 to 0.85 mm, which is the blank thickness for the present samples. The mesh consists of linear 8-node hexagonal (brick) reduced-integration elements with hourglass control. The yield locus uses a 6th-degree FACET formulation based on the ALAMEL or FC Taylor model with 5000 orientations.

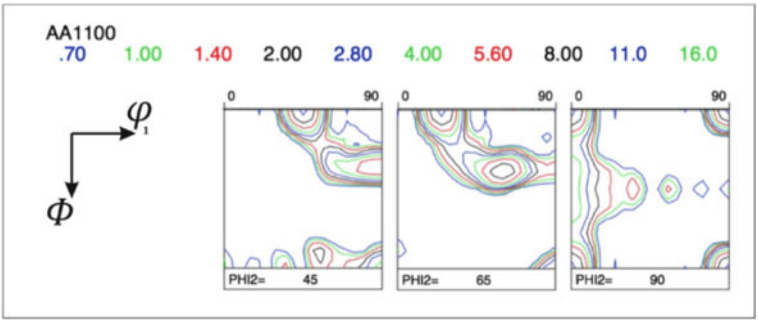

Fig. 1 φ_2 = constant sections of the ODF of the AA1100-alloy

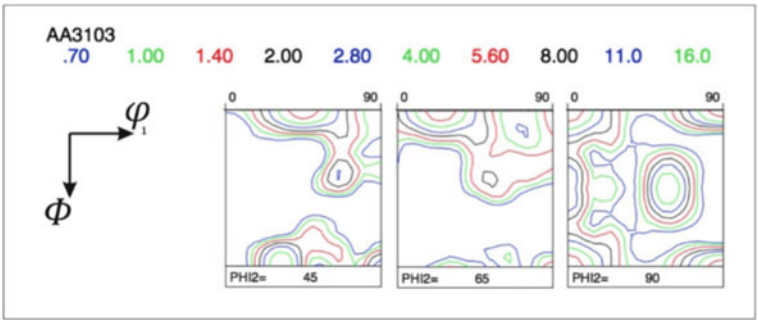

Fig. 2 $\varphi_2 =$ constant sections of the ODF of the AA3103-alloy

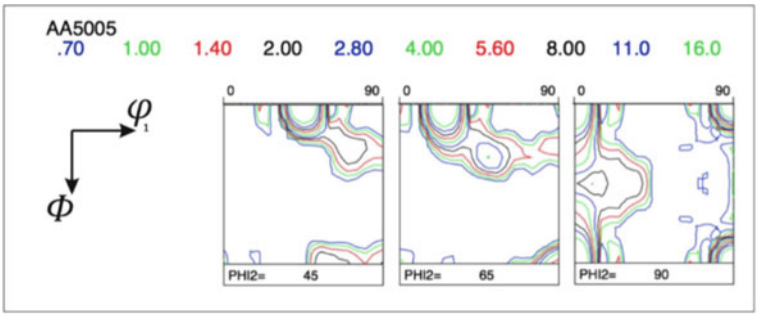

Fig. 3 $\varphi_2 =$ constant sections of the ODF of the AA5005-alloy

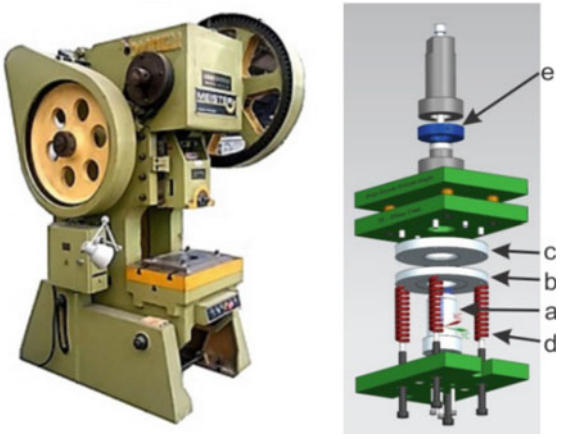

Fig. 4 Press and tool assembly. **a** Punch; **b** Blank holder; **c** Die; **d** Springs; **e** Load cell

3 Data Analysis

The measurement cloud obtained with the CMM does not coincide with the nodes of the deformed FEM-mesh (Fig. 5). To analyze the measurements, a cylindrical coordinate system (r,θ,z) is used. The minimum of the Z-coordinate, at the bottom of the cup, is set equal to 0 by a rigid body translation; points below a threshold height h_0 (typically 2.2 mm) are removed, i.e., only the cup walls are analyzed. Outliers are removed, and the measurement cloud is rotated to move its central axis into vertical position.

The corrected dataset is sliced vertically into sections of width $\Delta\theta$ (typically 1°). A polynomial fit of the radial distance between wall and center line is made for each slice using the following equation:

$$r(\theta_m, z) = \sum_{n=0}^{N} a_{mn} z^n \tag{1}$$

where θ_m is the central angle of the m^{th} segment and N the degree of the polynomial. In the first step, all points in the slice are used, which defines the central line of the wall segment. Then, the fit is made separately to the points inside and outside this central line, to fit the inner and outer surfaces producing a set of $360/\Delta\theta$ values a_{mn}^{ext} and a_{mn}^{int}. The values of the polynomial coefficients in Eq. (1) are fitted by a Fourier series:

$$a_n^p(\theta) = \sum_{l=0}^{L} c_{ln}\cos(l\theta) + \sum_{l=1}^{L} d_{ln}\sin(l\theta) \tag{2}$$

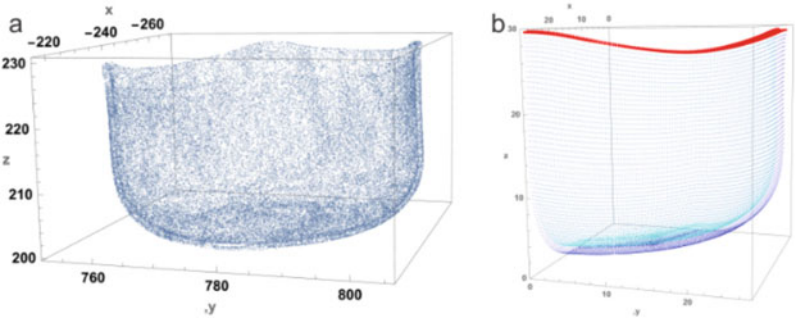

Fig. 5 **a** Measurement cloud obtained from CMM (only 1/10th of 482 269 points are plotted). **b** Surface nodes of the FEM model of one quarter of the cup, assuming orthotropic symmetry

The superscript p stands for the inner ($p = int$) and outer ($p = ext$) surface. The rim is detected as the highest point in each vertical slice on inner and outer surface. The average of both values is then fitted by a Fourier series for the rim height $h(\theta)$:

$$h(\theta) = \sum_{l=0}^{L} c_l \cos(l\theta) + \sum_{l=1}^{L} d_l \sin(l\theta) \tag{3}$$

Note that c_0 gives the average cup height. The cup is described by:

$$\begin{cases} r^p(\theta, z) = \sum_{n=0}^{N} a_n^p(\theta) r^n \\ h_0 < z < h(\theta) \end{cases} \tag{4}$$

The second line in Eq. 4 is essential to avoid extrapolation. Too low values of N and L produce a poor fit, too high values will introduce spurious undulations. Here, $N = L = 6$. The same fitting procedure is used for the nodes of the FEM-mesh, with orthotropic symmetry imposed in Eq. 3 by including only terms in $\cos(2lq)$.

Two corrections are made to the measured data. Asymmetry due to an eccentric positioning of the blank is mostly eliminated by setting the terms for $l = 1$ equal to 0. Small alignment errors between the rolling direction of the blank and the $\theta = 0$ direction in the CMM can be removed by adding a correction $\delta\theta$ to θ. However, even after these corrections, deviations of orthotropic symmetry are sometimes still observed. The measured rim height is symmetrized by the following operation [8]:

$$h_{Crr}(\theta) = \frac{h(\theta + \delta\theta) + h(-\theta) + h(\pi + \theta + \delta\theta) + h(\pi - \theta + \delta\theta)}{4} \tag{5}$$

4 Results and Discussion

The measured and modeled cups for AA5005 are shown in Fig. 6. The morphology of the rim, both in terms of radius and height, is very satisfactory. A more detailed comparison of the rim height profile is found in Fig. 7 for AA1100, Fig. 8 for AA3103, and Fig. 9 for AA5005. A first observation is that the FEM results overestimate the cup height by approximately 3mm. This may be due to the consideration of a constant blank holder force, as opposed to the variable force exercised by the springs, inaccuracies of the model in the bending zone at the punch radius at the bottom of the cup or an underestimation of the friction coefficient.

Strain rate sensitivity is not considered in the simulations. The deformation speed in the industrial press is much higher than on a laboratory rig for the Swift test. In turn, the strain rate in the laboratory test is higher than the one defined in ISO 6892–1:2016 for the tensile test. In aluminum alloys, this effect may be significant. Other factors which may affect the earing height in AA1100 and the small deviations in

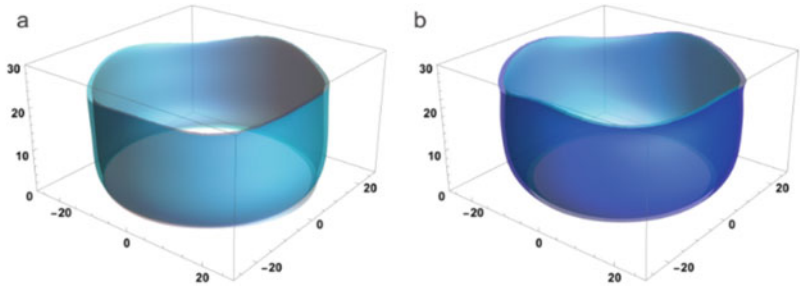

Fig. 6 AA5005. **a** CMM result, **b** FEM result. Good qualitative similarity is observed

Fig. 7 Cup profile as predicted by FEM and height-corrected measured profile for AA1100

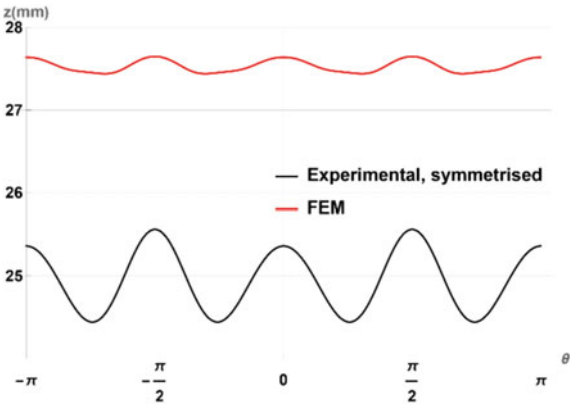

Fig. 8 Cup profile as predicted by FEM and height-corrected measured profile for AA3103

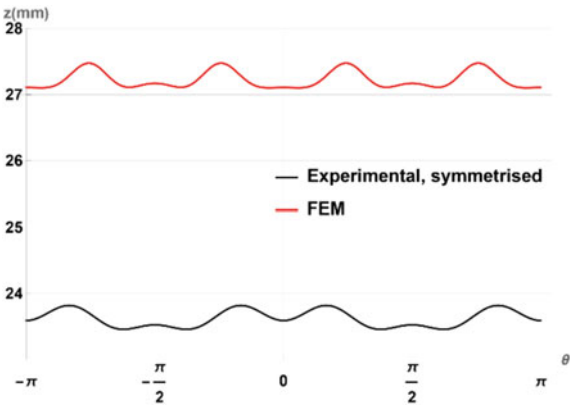

peak positions for AA3103 are the discretization procedure used to select the 5000 orientations used in the simulations, or fundamental effects of the crystal plasticity approach used.

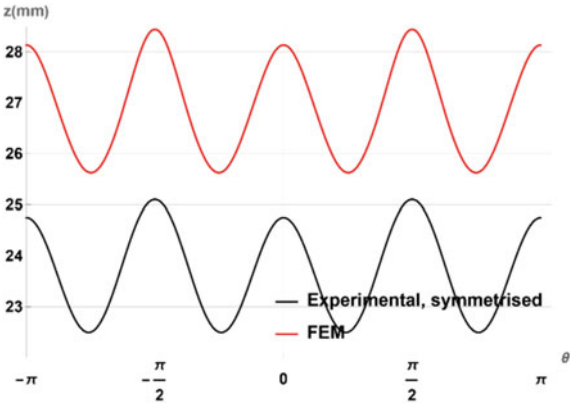

Fig. 9 Cup profile as predicted by FEM and height-corrected measured profile for AA5005

5 Conclusions

A cup drawing test was successfully developed on an industrial mechanical drawing press and full-field measurements of the deformed geometry were obtained with a mechanical-optical coordinate measurement machine. A Fourier-series fitting technique was developed to compare the measured data to FEM results.

Differences in strain rate, blank holder force and friction coefficient between the mechanical press and existing laboratory testing equipment induce challenges, which are unrelated to the theoretical approaches in the anisotropic plasticity codes. Further research on the effect of non-texture-related modeling parameters is required to enable a more precise evaluation of the theoretical models used in the FEM analysis.

The strong overestimation of the earing profile for the AA1100-alloy probably is an effect of the crystal plasticity models used or may be an effect of texture discretization, although the detailed reason for this discrepancy is difficult to identify. For the AA3103 and AA5005, coincidence between experiment and model is excellent, indicating that the modeling approach used here is highly reliable in most cases.

Finally, for AA1100 and AA3103, the earing amplitude is small. This imposes the need for a statistical evaluation of the measurement precision, in terms of eccentricity and misalignment of samples, to provide an estimation of the relative importance of modeling assumptions and statistical spread of experimental results.

Acknowledgements D.R.P., M.A.R., and R.S. acknowledge support from DGAPA grant IN113123 during the final stages of this project. D.R.P. acknowledges his scholarship by CONACYT for his master's studies.

References

1. Dixit US (2020) Modeling of metal forming: a review. Mechanics of materials in modern manufacturing methods and processing techniques, pp 1–30
2. Van Houtte P, Gawad J, Eyckens P, Van Bael A, Samaey G, Roose D (2011) A full-field strategy to take texture induced anisotropy into account during FE simulations of metal forming processes. J Metals 63:37–43
3. Banabic D, Barlat F, Cazacu O, Kuwabara T (2020) Advances in anisotropy of plastic behaviour and formability of sheet metals. IntJ Mater Form 13:749–787
4. Habraken AM, Aksen TA, Alves JL et al (2022) Analysis of ESAFORM 2021 cup drawing benchmark of an Al alloy, critical factors for accuracy and efficiency of FE simulations. IntJ Mater Form 15(5):61
5. Clarke AP, Van Houtte P, Saimoto S (1994) Mater Sci Forum 157–162:1953
6. Van Houtte P, Clarke P, Saimoto S (1993) A quantitative analysis of earing during deep drawing. In: Morris JG et al. (eds), Aluminum alloys for packaging, TMS, 261
7. Hosford WF, Caddell RM (2011) Metal forming: mechanics and metallurgy. Cambridge University Press
8. Schouwenaars R, Van Houtte P, Van Bael A, Winters J, Mols K (1996) Analysis and prediction of the earing behaviour of low carbon steel sheet. Textures Microst 27:553–570
9. Van Houtte P, Li S, Seefeldt M, Delannay L (2005) Deformation texture prediction: from the Taylor model to the Advanced Lamel model. Int J Plast 21:589–624
10. Engler O, Kalz S (2004) Simulation of earing profiles from texture data by means of a visco-plastic self-consistent polycrystal plasticity approach. Mater Sci Eng A, A 373:350–362
11. Engler O, Hirsch J (2007) Polycrystal-plasticity simulation of six and eight ears in deep-drawn aluminum cups. Mater Sci Eng A, A 452:640–651
12. Van Houtte P, Van Bael A, Winters J (1995) The incorporation of texture-based yield loci into elasto-plastic finite element programs. Textures Microstr 24(4):255–272
13. Munhoven S, Habraken AM, Winters J, Schouwenaars R, Van Houtte P (1995) Application of an anisotropic yield locus based on texture to a deep drawing simulation. In: Proceedings Numiform 1995, 5th international conference on numerical methods in industrial forming processes, pp 767–772. Balkema, Rotterdam
14. Barlat F, Aretz H, Yoon JW, Karabin M, Brem JC, Dick R (2005) Linear transfomation-based anisotropic yield functions. Int J Plast 21(5):1009–1039
15. Yoon JW, Barlat F, Chung K, Pourboghrat F, Yang DY (2000) Earing predictions based on asymmetric nonquadratic yield function. Int J Plast 16:1075–1104
16. Yoon JW, Barlat F, Dick RE, Karabin ME (2006) Prediction of six or eight ears in a drawn cup based on a new anisotropic yield function. Int J Plast 22:174–193
17. Yoon JH, Cazacu O, Yoon JW, Dick RE (2010) Earing predictions for strongly textured aluminum sheets. Int J Mech Sci 52(12):1563–1578
18. Han F, Diehl M, Roters F, Raabe D (2020) Using spectral-based representative volume element crystal plasticity simulations to predict yield surface evolution during large scale forming simulations. J Mater Process Technol 277:116449
19. Roters F, Diehl M, Shanthraj P, Eisenlohr P, Reuber C, Wong SL, Maiti T, Ebrahimi A, Hochrainer T, Fabritius HO, Nikolov S (2019) DAMASK–The Düsseldorf Advanced Material Simulation Kit for modeling multi-physics crystal plasticity, thermal, and damage phenomena from the single crystal up to the component scale. Comput Mater Sci 158:420–478
20. Gawad J, Van Bael A, Eyckens P, Samaey G, Van Houtte P, Roose D (2013) Hierarchical multi-scale modeling of texture induced plastic anisotropy in sheet forming. Comput Mater Sci 66:65–83
21. Ramírez MA, Schouwenaars R, Eyckens P, Gawad J, Kestens L, Van Bael A, Van Houtte P (2016) Experimental validation and effect of modelling assumptions in the hierarchical multi-scale simulation of the cup drawing of AA6016 sheets. Modell Simul Mater Sci Eng 25(1):015002

22. Van Houtte P, Yerra SK, Van Bael A (2009) The Facet method: a hierarchical multilevel modelling scheme for anisotropic convex plastic potentials. Int J Plast 25:332–360
23. Van Houtte P (1984) A new method for the determination of texture functions from incomplete pole figures—comparisons with older methods. Textures Microst 6:137–162
24. Bunge HJ (1982) Texture analysis in materials science. Butterworth's, London